The Journal of Chemical Physics

Light-induced processes in nature: Coherences in the establishment of the nonequilibrium steady state in model retinal isomerization

Cite as: J. Chem. Phys. **150**, 184304 (2019); https://doi.org/10.1063/1.5092981
Submitted: 15 February 2019 • Accepted: 23 April 2019 • Published Online: 13 May 2019

Amro Dodin and Paul Brumer

The Journal of Chemical Physics ARTICLE scitation.org/journal/jcp

Light-induced processes in nature: Coherences in the establishment of the nonequilibrium steady state in model retinal isomerization

Cite as: J. Chem. Phys. 150, 184304 (2019); doi: 10.1063/1.5092981
Submitted: 15 February 2019 • Accepted: 23 April 2019 •
Published Online: 13 May 2019

Amro Dodin[a] and Paul Brumer[b]

AFFILIATIONS

Chemical Physics Theory Group, Department of Chemistry, and Center for Quantum Information and Quantum Control, University of Toronto, Toronto, Ontario M5S 3H6, Canada

[a]**Current address:** Department of Chemistry, Massachusetts Institute of Technology, Cambridge, Massachusetts 02139, USA.
[b]**Author to whom correspondence should be addressed:** paul.brumer@utronto.ca

ABSTRACT

Dynamics and coherences in retinal isomerization are investigated in a standard two-mode two-state model irradiated by natural incoherent light using the Markovian partial-secular Bloch-Redfield formalism. The two-mode two-state model is a minimal model of retinal that considers vibronic states on a ground and excited electronic manifold coupled to two continuous Ohmic harmonic baths. All light-induced coherent oscillations are shown to disappear as the turn-on time becomes realistically slow. Rather, an interplay between incoherent-light induced coherences and environmentally induced coherences is exposed as the system approaches a nonequilibrium steady state. The dynamics of the system reveal stable steady state coherences under realistic conditions, producing a small but robust transient enhancement of quantum yield.

I. INTRODUCTION

Light-induced processes are ubiquitous in nature, where specialized biomolecules, such as photosynthetic light harvesting complexes and rhodopsins in visual centers, display remarkable photophysical properties tuned to their biochemical roles.[1–5] This has spurred a series of increasingly sophisticated coherent laser experiments that use short light pulses to initiate and probe the fs dynamics of the process of interest.[6–15] Paired with detailed theoretical modeling, the observed short-time dynamics has elucidated the structure and energetics of these biochromophores and their protein environments.[3,16–22] However, in nature, biomolecular processes are initiated and maintained by incoherent light, e.g., sunlight, with dramatically different molecular responses.[23–35] Treating the dynamics of systems illuminated by natural light poses a significant challenge to describing light-induced processes in a realistic setting. In particular, understanding the nature and role of quantum coherences, which describe the relative phase between system energy eigenstates, remains a central issue in the goal of identifying nontrivial quantum effects in biological processes.

In this study, we examine a significant example of biomolecular dynamics driven by slowly turned-on incoherent light that reflects the fields they experience in nature. We describe the requirements and physical origin of the different types of coherences that can arise in light-induced molecular processes. By considering the example of retinal photoisomerization, the first step in vision, we illustrate the role played by coherences in a realistic biological system and expose generic features that are manifest in a wide range of light-induced processes in biology. We find that previously reported light-induced coherences do not survive under natural illumination conditions. Instead, the interplay between the incident light and protein environment generates a new form of robust two-bath coherence. These *transport-induced coherences* are established and maintained by the continuous transfer of energy from the high temperature photon bath to the low temperature phonon bath through the molecular system. In retinal, transport-induced coherences produce a small but robust transient enhancement of the photoisomerization quantum yield, and are surprisingly associated with a coherent nonequilibrium steady state (NESS). This suggests that, while they may differ drastically from the coherent dynamics

observed in laser experiments, quantum effects may play a role in biological systems under realistic conditions.

The search for quantum effects in biology was recently sparked by the observation of long-lived oscillatory coherences in laser-driven photosynthetic complexes.[8–10,12] This led to widespread theoretical and experimental efforts that described the transport of coherent excitations through multichromophoric biomolecules,[6,11,16,36,37] proposed methods for exploiting quantum coherence to engineer more active photovoltaic devices[7,38] and probed photoprotection mechanisms in biomolecules.[14] In addition we, as well as other groups, examined the nature of excitations generated by natural incoherent light and how they differ from those prepared by laser light.[23,25,28,29,33–35,39–43] These studies found that incoherent driving of biomolecules generates a different form of coherences than those seen in laser experiments. These noise-induced coherences had been previously proposed in quantum optical studies of atomic systems[31,32,44–46] and differ significantly from those excited by coherent light in their dynamics and physical origin. Several proposals have been put forward for exploiting these coherences to enhance the efficiency of energy harvesting in noise-driven systems,[47,48] suggesting that biological systems may exploit similar physics for their remarkable efficiency.[33,49]

These studies assumed, however, that the incident light was turned-on instantly, suddenly jarring the system out of equilibrium. This behavior is distinctly different from natural settings where light intensities are modulated extremely slowly on molecular time scales. As a consequence, we, more recently, considered the dynamics of molecules under more realistic turn-on conditions[27,28] and have found that even these noise-induced coherences are suppressed when the light intensity rises slowly. Biomolecular dynamics is often much richer than that of the simple models studied, containing many more states and a protein-environment in addition to the driving light-field. This added complexity motivates this study of a more complicated model containing new physics associated with a slow turn-on.

As an illustrative example, we consider the photoisomerization of model retinal in rhodopsin. This system has several remarkable properties that contribute to the efficiency of vision and has been well characterized both experimentally and theoretically in the coherent excitation limit.[3,15,22] For example, retinal photoisomerization has a high quantum yield of 65% to the all-*trans* photoproduct,[50] and in pulsed laser experiments, formation of the all-*trans* product has been observed on the ultrafast sub-50 fs time scale.[15] Furthermore, computational studies show that the rhodopsin protein environment plays an important role in the enhancement of the quantum yield of retinal.[3,22]

These observations have led to studies into the potential role of quantum effects in retinal photoisomerization.[3,22,51,52] In the recent study of the excitation of retinal by incoherent light, in addition to dynamics that differed significantly from pulsed laser excitation, both a transient coherent enhancement of the quantum yield and stationary coherences were demonstrated, even under suddenly turned-on incoherent excitation, suggesting that quantum effects may play a role in the primary photoreaction in human vision.[52] However, as noted above, this study, as many others, assumed the instantaneous turn-on of the incoherent light, whereas natural turn-on times are extremely long on the molecular time scale. For example, blinking defines a natural turn-on time for retinal in the human eye and occurs on a time scale of ∽100 ms. By contrast, molecular dynamics can occur at least 11 orders of magnitude faster, on the order of 0.1–1 ps.[52]

The goal of this paper is to illustrate the nature and role of coherences in a model biomolecule excited by natural incoherent light. In Sec. II, we provide an account of the different types of coherences that arise in molecular photoexcitation, describing the physical origin of each and the conditions under which they play a significant role. First, the Partial Secular Bloch-Redfield (PSBR) formalism used in this study is presented in Sec. II A. Section II B and the Appendix briefly review previously reported light-induced coherences and provide a novel semiclassical description of their generation that allows for an intuitive comparison to laser-induced coherences. The physics introduced by the addition of a protein environment is then outlined in Sec. II C, describing how nonradiative relaxation is influenced by coherences and can generate them. In Sec. II D, we show how introducing a second bath can break constraints imposed by fluctuation-dissipation relations, leading to transport-induced coherences in the nonequilibrium steady state. The standard Two-State Two-Mode (2S2M) model of retinal is then presented in Sec. III, and the resulting interplay of coherences in retinal photoisomerization is described in Secs. IV and V. We conclude by summarizing the finding of this study and outlining the potential implications of these coherences in general biological systems in Sec. VI.

II. INCOHERENT EXCITATION OF BIOMOLECULES

Consider the dynamics of an incoherently driven biomolecule embedded in a protein environment. Neglecting any interactions between the light and the vibrational modes of the protein, this system can be modeled by a Hamiltonian of the form

$$\hat{H} = \hat{H}_S + \hat{H}_{rad}(t) + \hat{H}_{ph} + \hat{H}_{S-rad} + \hat{H}_{S-ph}, \tag{1}$$

where $\hat{H}_S$ gives the unperturbed energy of the subsystem and $\hat{H}_{rad}(t)$ and $\hat{H}_{ph}$ describe the energetics of the incoherent light and phonon modes of the protein, respectively. The time-dependence of $\hat{H}_{rad}(t)$ models an external environment attenuating the intensity of incident light and generates its turn-on behavior.[28] The system interacts with the radiative and phonon environments through interaction Hamiltonians $\hat{H}_{S-rad}$ and $\hat{H}_{S-ph}$, respectively.

A system modeled by such a Hamiltonian then evolves under the following Quantum Master Equation (QME):

$$\frac{d}{dt}\hat{\rho} = -\frac{i}{\hbar}\left[\hat{H}_S, \hat{\rho}\right] + \hat{\hat{\mathcal{L}}}_{rad}(t)\hat{\rho} + \hat{\hat{\mathcal{L}}}_{ph}[\hat{\rho}]\,, \tag{2}$$

where the reduced density matrix, $\hat{\rho} = \mathrm{Tr}_{rad}\mathrm{Tr}_{ph}\hat{\rho}_{full}$, is obtained by tracing the full density matrix, $\hat{\rho}_{full}$, over the radiation (Tr_{rad}) and phonon baths (Tr_{ph}). The first commutator, $\hat{\hat{\mathcal{L}}}_0 := -i/\hbar\left[\hat{H}_S, \cdot\right]$, describes the unitary evolution of the closed retinal system, and the subsequent Liouvillians contain the nonunitary evolution induced by the time-dependent light and by the phonon environment, respectively.

The form of Eq. (2) can be used to study both Markovian and non-Markovian dynamics. Recent methodological advances have enabled the study of non-Markovian effects in complex systems,[19,20,53] providing more accurate descriptions of the phonon

bath induced dynamics. However, these approaches lead to equations that are much more complex than their Markovian counterparts, complicating the description of the simple physical mechanisms that generate coherence in biomolecular systems. Moreover, non-Markovian effects are expected to be small for systems that are weakly coupled to an environment with short correlation time.[54,55]

With suitable models for the biomolecular subsystem, incoherent light, and the protein environment, Eq. (2) can be numerically integrated[52] to obtain the quantum dynamics of incoherently driven biomolecules. In the remainder of this section, we first consider each of the Liouvillians in Eq. (2) in order to characterize the coherences generated by the two baths separately. We then treat the interplay of the two baths that generates transport-induced coherence.

A. Partial secular Bloch-Redfield equations

The photon field Hamiltonian is given by $\hat{H}_{rad} = \sum_{\boldsymbol{k}\lambda} \hbar\omega_k \hat{a}_{\boldsymbol{k}\lambda}\hat{a}^{\dagger}_{\boldsymbol{k}\lambda}$ where ω_k is the frequency of the field mode with wave vector $\boldsymbol{k}$ and polarization λ and $\hat{a}_{\boldsymbol{k}\lambda}$ and $\hat{a}^{\dagger}_{\boldsymbol{k}\lambda}$ are the corresponding annihilation and creation operators. The system-radiation interaction Hamiltonian is given, in the dipole approximation, by

$$\hat{H}_{S-rad} = -\boldsymbol{\mu}\sum_{\boldsymbol{k}\lambda}\left(\frac{\hbar\omega_k}{2\epsilon_0 V}\right)^{\frac{1}{2}}\epsilon_{\boldsymbol{k}\lambda}\left(\hat{a}_{\boldsymbol{k}\lambda} - \hat{a}^{\dagger}_{\boldsymbol{k}\lambda}\right). \tag{3}$$

Here, the dipole moment is given by $\boldsymbol{\mu}$, and the polarization vector of the field mode with wavevector $\boldsymbol{k}$ and polarization λ is given by $\boldsymbol{\epsilon}_{\boldsymbol{k}\lambda}$.

The Liouvillian for the system-radiation field interaction can be obtained using the PSBR formalism[26,29] and its generalization to time varying fields.[28] This is given by

$$\begin{aligned}(\hat{\hat{\mathcal{L}}}_{rad}(t)\hat{\rho})_{ij} = {} & p_{ij}\sqrt{r_i(t)r_j(t)}\rho_{gg}(t) \\ & - \frac{1}{2}\sum_k p_{ik}\left(\sqrt{\gamma_i\gamma_j} + \sqrt{r_i(t)r_j(t)}\right)\rho_{kj}(t) \\ & - \frac{1}{2}\sum_k p_{jk}\left(\sqrt{\gamma_j\gamma_k} + \sqrt{r_j(t)r_k(t)}\right)\rho_{ik}(t),\end{aligned} \tag{4}$$

where $r_i(t) = B_i W(\omega_{ge_i};t)$ is the incoherent pumping rate from the ground state $|g\rangle$ to the excited state $|e_i\rangle$, which depends on the instantaneous energy density of the incoherent light field $W(\omega_{ge_i};t)$ and the Einstein B-coefficient $B_i = \pi|\mu_{ge_i}|^2/3\epsilon_0$. Here, $\gamma_i = \omega^3_{ge_i}|\mu_{ge_i}|^2/3\pi\epsilon_0 c^3$ is the corresponding spontaneous emission rate. The energy difference between excited states $|e_i\rangle$ and $|e_j\rangle$ is denoted by ω_{ij}. The parameters $p_{ij} = \boldsymbol{\mu}_{ge_i}\cdot\boldsymbol{\mu}_{ge_j}/|\mu_{ge_i}||\mu_{ge_j}|$ are a measure of the alignment between the $|g\rangle \leftrightarrow |e_{i,j}\rangle$ transition dipole moments. The incoherent pumping and spontaneous emission rates are related by the fluctuation-dissipation relation to give $r_i(t) = \gamma_i\bar{n}(\omega_0;t)$, where $\bar{n}(\omega_0;t)$ is the time dependent mean occupation of the radiation field at the ground to bright state transition frequency $\omega_0 \gg \omega_{ij}$.[56] The slow turn-on of the radiation field manifests through the time dependence of $\bar{n}(\omega_{ij};t)$, which we take to be of the form $\bar{n}(\omega_0;t) = \bar{n}(\omega_0)(1 - e^{-t/\tau_r})$, where $\bar{n}(\omega_0) = \lim_{t\to\infty}\bar{n}(\omega_0;t)$ is the steady-state occupation number and τ_r is the turn-on time of the radiation field. In the case of natural excitation of retinal, the light-field is extremely weak and satisfies a weak pumping limit $r_i(t)/\gamma_i \ll 1$ at all times.

Equation (4) describes the generation of light-induced coherences upon excitation from the ground state (in the first term) and the coupling between populations and coherences through interference and vacuum-induced coherences (in the remaining terms).[29,31,32,34,44,46,57] The rate of initial coherence generation is set by the incoherent pumping rate $r_i(t)$ and consequently shows a significant time dependence. By contrast, due to the low intensity of natural light, spontaneous decay processes with time-independent rates γ_i dominate over stimulated emission contributions to the light-induced coherences and interference effects. In addition, the dipole alignment p_{ij} sets the strength of population-coherence coupling and can be used to tune the generation of light-induced coherences. This provides a convenient method of artificially suppressing light-induced coherences, i.e., by setting $p_{ij} = \delta_{ij}$, allowing for the study of retinal dynamics where excitation with light does not induce coherences. We exploit this below to isolate phonon-induced, i.e., vibrationally induced, coherences in retinal.

B. Light-induced coherence

Consider now the physical origin of noise-induced coherences described by Eq. (4). These Fano coherences were first observed in quantum optical studies of atomic excitation.[31,32,44–46] Consequently, they are typically described using a quantum description of the incident light, where simultaneous absorption of two virtual photons establishes coherence between two states. However, we have also seen noise-induced coherences in a semiclassical study[27] where the exciting field is treated as classical noise, indicating that a semiclassical mechanism describing their origin is possible. Such a picture would provide further insight into the physical source of coherence induced by noisy light and enable more intuitive comparisons to laser-induced coherences. In particular, a semiclassical description would reveal the role of the phase statistics of the driving field in determining the coherence of the material system upon which it is incident.

To do this, consider a simple model of the incident light with the driving field having a time-varying intensity and phase

$$E^{+}(t) = A(t)e^{-i\phi(t)}. \tag{5}$$

Here, the intensity is given by $I = A^2(t)$ and both the field magnitude $A(t)$ and phase $\phi(t)$ are real valued. We note that this is related to the usual frequency domain field description, $E^{+}(t) = \int d\omega \tilde{A}(\omega)e^{-i\phi(\omega)}e^{-i\omega t}$, by a Fourier transform.

Equation (5) can be used to describe most classical fields. For example, coherent continuous wave lasers generate a field with constant magnitude A and $\phi(t) = \omega t$, while an instantaneous laser pulse at time t_0 is given by $A(t) = \delta(t - t_0)$ with a freely selected phase $\phi(t_0)$. By contrast, incoherent or partially coherent light can be described by treating the phase as a time-dependent random variable. A simple method for quantifying the degree of coherence of partially coherent light can be defined for fields with phases that obey an exponential correlation function $\langle\phi(t_0)\phi(t + t_0)\rangle = \exp(-t/\tau_c)$. In such a system, the correlation time of the phase gives the coherence time of the incident field. This generalizes a related numerical approach to partially coherent light that unravels it into an ensemble of piecewise continuous wave realizations with random phase jumps.[24,58]

Equipped with a semiclassical description of the driving field, consider its interaction with a material system. Molecular response to an electromagnetic field can be expanded into an asymptotic perturbation (e.g., similar to the PSBR formalism in Sec. II A). This expresses light-induced dynamics as a sum over discrete interactions occurring at times $\{t_i\}$ interspersed with unitary system evolution, as described in the Appendix. This approach is effective for systems weakly coupled to the incident light and is the standard method used to study natural excitation conditions and most laser-induced experiments.[23,55,59,60]

To illustrate the physical origin of Fano coherences, we treat the simplest interaction capable of generating a coherent superposition. Consider a system initially in ground state $|g\rangle$ with energy $\epsilon_0 = 0$. At t_1, it interacts with a semiclassical field described by Eq. (5), inducing a transition to state $|1\rangle$ with energy ϵ_1. Then, at some later time t_2, it interacts again with the field, inducing a transition from $|g\rangle$ to state $|2\rangle$ with energy ϵ_2. The relative phase between the two states $|1\rangle$ and $|2\rangle$ at some time $t > t_2 > t_1$ is then given by (see the Appendix)

$$\Delta\phi_{12}(t;t_1,t_2) = \phi(t_2) - \phi(t_1) + \frac{(\epsilon_2-\epsilon_1)}{\hbar}(t-t_2) - \frac{\epsilon_1}{\hbar}(t_2-t_1). \tag{6}$$

For incoherent excitations, $\phi(t_2)$ and $\phi(t_1)$ are uncorrelated for all $t_2 \neq t_1$. That is, in these systems, $\phi(t_2) - \phi(t_1)$ is a uniform random variable in the range $[-\pi, \pi)$. As a result, the coherence contribution from these interactions $\rho_{12}(t;t_1,t_2) \sim \langle \exp(-i\Delta\phi_{12}(t;t_1,t_2))\rangle$ vanishes for all nonsimultaneous excitations ($t_1 \neq t_2$). By contrast, for coherent excitation $\phi(t_2)$ and $\phi(t_1)$ are deterministic variables, generating a pure-state superposition between states $|1\rangle$ and $|2\rangle$. For $t_2 = t_1$, however, the exciting field generating both transitions has the same phase, giving $\phi(t_2) - \phi(t_1) = 0$ regardless of the coherence time of the driving field. As such, these simultaneous excitations are identical for coherent and incoherent sources and are responsible for the generation of noise-induced coherence. This indicates that a small subset of interactions generated by incoherent light act identically to their laser driven analogs. The remainder of excitations with $t_1 \neq t_2$ contributes no coherence and can therefore be neglected.

An interesting property emerges when considering excitation by a light field that is turned on at $t = t_0$. More concretely, consider a field with some time t_0 such that $A(t) = 0$ if $t < t_0$. At the instant t_0 when the light field begins to turn-on, t_1 and t_2 can only take one value, $t_1 = t_2 = t_0$, since the intensity of the field is zero for all $t < t_0$. Remarkably, then, at this instant, coherent excitation and incoherent excitation cannot be distinguished since the fluctuating phase of incoherent light has not yet manifested. As a result, initial excitation by one field mode of incoherent light is fully coherent. We have observed this behavior in previous studies of noise-induced coherence[26,28,51] and is also seen in the photoexcitation of retinal below.

In addition, unpolarized incoherent light in three dimensions has two independent polarization modes that can drive molecular transitions. The phase of these modes is uncorrelated; therefore, if each of the transitions discussed above is generated by a different polarization mode, even simultaneous excitation will produce no coherence. Consequently, coherences are only generated by excitations driven by the same polarization mode. The probability of two states being driven by the same polarization mode is given by the angle between their transition dipole moments and is controlled by the parameter p_{ij} discussed in Sec. II A. As such, noise-induced coherences can be generated between states with $p_{ij} \neq 0$. However, if the turn-on is slower than the lifetime of these coherences, they do not build up appreciably in the system. This leads to the loss of coherence dynamics occurring on time scales slower than the turn-on time of light.[27,28]

C. Vibration-induced relaxation

The phonon bath of intramolecular and environmental vibrations can be modeled by the harmonic Hamiltonian $\hat{H}_{ph} = \sum_{\alpha,n} \omega_{\alpha,n} \hat{b}^\dagger_{\alpha,n} b_{\alpha_n}$. This bath interacts linearly with the molecular system through

$$\hat{H}_{S-ph} = \sum_\alpha \hat{A}_\alpha \hat{B}_\alpha, \tag{7}$$

where α denotes the independent modes coupled to the system degrees of freedom (e.g., analogously to polarization modes in light). The system modes $\hat{A}_\alpha$ couple to the phonon bath modes $\hat{B}_\alpha = \sum_n \lambda_{\alpha,n}(\hat{b}_{\alpha,n} + \hat{b}^\dagger_{\alpha,n})$, where $\lambda_{\alpha,n}$ is the coupling of system mode α to the nth phonon mode. These coupling coefficients define the spectral density of the bath modes, which defines the interaction between the system and phonon environment.

The resulting contribution to the density matrix dynamics is described, in the Redfield formalism, by the Liouvillian[21,61]

$$\left(\hat{\mathcal{L}}_{ph}\hat{\rho}\right)_{ij} = \sum_{kl} \mathcal{R}_{ijkl}\rho_{kl}(t), \tag{8}$$

where each degree of freedom ($\alpha = \phi, x$) is assumed to be coupled to its own independent harmonic oscillator bath.[21] The Redfield tensor elements are given by[21,54,61]

$$\mathcal{R}_{ijkl} = \sum_\alpha \left[-\delta_{lj} \sum_r \Gamma^{(+)\alpha}_{irrk} - \delta_{ik} \sum_r \Gamma^{(-)\alpha}_{lrrj} + \Gamma^{(+)\alpha}_{ljik} + \Gamma^{(-)\alpha}_{ljik} \right], \tag{9}$$

in terms of the spectral correlation tensor, $\Gamma^{(\pm)\alpha}$, with[52]

$$\Gamma^{(+)\alpha}_{ljik} = \frac{1}{2\pi} A^\alpha_{lj} A^\alpha_{ik} B^{(+)\alpha}_{ik}, \tag{10}$$

where $A^\alpha_{lj} = \langle l|\hat{A}_\alpha|j\rangle$ and

$$B^{(+)\alpha}_{ik} \approx \Re\left(B^{(+)\alpha}_{ik}\right) = \begin{cases} \pi J_\alpha(\omega_{ik}) n(\omega_{ik}), & (\omega_{ik} > 0), \\ \pi J_\alpha(|\omega_{ik}|)[1 + n(\omega_{ik})], & (\omega_{ik} < 0), \end{cases} \tag{11}$$

where $n(\omega) = [e^{\hbar\omega/kT} - 1]^{-1}$ is the Bose distribution at temperature T. The small Lamb shift contained in the imaginary part of the coefficient $B^{(+)\alpha}_{ik}$ has been neglected. The fluctuation-dissipation relationship between $B^{(+)\alpha}_{ik}$ for excitations ($\omega_{ik} > 0$) and emission ($\omega_{ik} > 0$) in Eq. (11) is analogous to that seen in light-induced coherences and similarly guarantees that a system driven by the phonon bath will evolve into a thermal steady state.

The Redfield relaxation tensor defined by Eqs. (9)–(11) contains five types of elements each describing a different physical process. Tensor elements, R_{ijkl}, with $i = j$ and $k = l$, couple the populations of energy eigenstates and give the rate of incoherent transitions (i.e., without interference) between them. By contrast, elements with

$i \neq j$ and $(i, j) = (k, l)$ describe coherence loss between states $|i\rangle$ and $|j\rangle$ due to entanglement with the phonon bath and phonon-induced dephasing. Interference between decay pathways couples coherences to population and manifests in terms with $i \neq j$ and $k = l$.

In addition to these familiar processes, there are two other contributions of particular interest to the study of incoherent excitation. Incoherent phonons can generate and transfer noise-induced coherences (which we refer to as vibration-induced coherences) through the same mechanisms as incoherent light. When two transitions are generated by simultaneous interactions with the same phonon mode, α, vibration-induced coherences can arise between the two target states k and l. If both transitions originate from the same initial state, i, the phonon driven transition generates a coherent superposition of states k and l producing vibration-induced coherence between them. This contribution is contained in the tensor element $\Gamma_{ii,kl}$. If, instead, the transitions originate from two different states, i and j, the simultaneous interaction will transfer coherence from state i and j. The resulting vibration-induced coherence transfer is described by the tensor element $\Gamma_{ij,kl}$. Both of these coherence generating and transferring interactions can only occur between states that can interact with the same environment mode α. Due to these last three contributions, the nonradiative decay dynamics of an excitation are highly sensitive to its coherences and can, for example, allow for the breaking of detailed balance.[33,47] More concretely, they cause different coherent superpositions of the bright states to relax into different intermediate and product states, altering the vibration-induced relaxation cascade.

This discussion reveals a complicated interplay between vibration and light-induced coherences, indicating that they cannot be considered separately. In particular, although each bath satisfies its own fluctuation-dissipation relations guaranteeing that a system in contact with only one bath will reach a thermal equilibrium steady state, the two baths are at different temperatures. This leads to a system where the overall transition rates do not satisfy a fluctuation-dissipation relation. Consequently, such a system may display steady state coherences that would survive the slow turn-on limit.

D. Transport-induced coherences

In order to demonstrate how the overall breaking of fluctuation-dissipation relations leads to a coherent NESS, we consider a simple analytically tractable model system shown in Fig. 1. A three level V-system with ground state $|g\rangle$ and excited states $|e_1\rangle$ and $|e_2\rangle$ interacts with a radiative photon bath and a nonradiative phonon bath. The ground and excited state manifolds are separated by a transition frequency ω_0, while the two excited states are separated by an energy $\Delta = \hbar\omega_{12}$, where ω_{12} is the transition frequency between $|e_1\rangle$ and $|e_2\rangle$. The photon bath drives absorption and stimulated emission between $|g\rangle$ and $|e_i\rangle$ with incoherent pumping rate r_i and drives spontaneous emission at a rate γ_i. Similarly, the nonradiative bath drives absorption and stimulated emissions between these states with pumping rate R_i, spontaneous emission rate Γ_i, and a dephasing rate Γ_D. In addition, the radiative and nonradiative baths have "transition alignment" parameters p and P, respectively, proportional to the probability of each bath inducing simultaneous transitions between $|g\rangle$ and $|e_1\rangle$ and between $|g\rangle$ and $|e_2\rangle$. For dipole mediated transitions driven by an isotropic field, these are given in terms of the alignment of $\boldsymbol{\mu}_{ge_i}$, the $|g\rangle \leftrightarrow |e_i\rangle$ transition dipole moments, by $p = \boldsymbol{\mu}_{ge_1} \cdot \boldsymbol{\mu}_{ge_2} / \mu_{ge_1}\mu_{ge_2}$. This alignment term quantifies the probability of simultaneous light-induced $|g\rangle \leftrightarrow |e_1\rangle$ and $|g\rangle \leftrightarrow |e_2\rangle$ transitions and provides a useful parameter that can be used to phenomenologically attenuate noise-induced coherences. Motivated by this, we define an analogous parameter P that gives the probability of simultaneous phonon-induced transitions which can similarly be used to tune vibration-induced coherence. As seen in Eq. (12), $P = 0$ corresponds to no coherence induced in the system by the phonon bath, whereas $P = 1$ corresponds to maximum phonon-induced coherence. Similar models were treated in Refs. 26, 29, 33, 34, and 42, but with an unrelated focus.

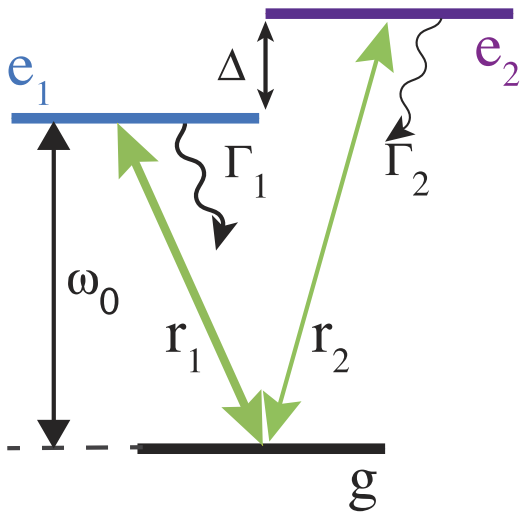

FIG. 1. Schematic illustration of an analytic Bloch-Redfield model for steady state coherences. The ground to excited state manifold splitting is given by a transition frequency ω_0, while splitting between the excited states is given by Δ. The incoherent photon bath drives absorption and stimulated emission between states $|g\rangle$ and $|e_i\rangle$ at a rate r_i, while the phonon bath drives nonradiative decay at a rate Γ_i.

In most molecular systems, nonradiative relaxation processes occur on time scales much faster than fluorescence; hence, it is reasonable to assume $\Gamma_i \gg \gamma_i$. The phonon bath in these systems is at far too low temperature to drive excitations between the ground and bright states and so $r_i \gg R_i$. In addition, dephasing can be included through an explicit rate Γ_D. Overall, this gives a V-system model pumped by the photon bath with rates r_i, while spontaneous relaxation is primarily driven by the nonradiative bath with relaxation rates Γ_i. This gives the following approximate PSBR master equations:

$$\dot{\rho}_{gg} = -(r_1 + r_2)\rho_{gg} + (r_1 + \Gamma_1)\rho_{e_1e_1} + (r_2 + \Gamma_2)\rho_{e_2e_2} + 2\left(p\sqrt{r_1 r_2} + P\sqrt{\Gamma_1\Gamma_2}\right)\rho^R_{e_1e_2}, \tag{12a}$$

$$\dot{\rho}_{e_ie_i} = r_i\rho_{gg} - (r_i + \Gamma_i)\rho_{e_ie_i} - \left(p\sqrt{r_1 r_2} + P\sqrt{\Gamma_1\Gamma_2}\right)\rho^R_{e_1e_2}, \tag{12b}$$

$$\dot{\rho}_{e_1e_2} = p\sqrt{r_1 r_2}\rho_{gg} - \frac{1}{2}\left(p\sqrt{r_1 r_2} + P\sqrt{\Gamma_1\Gamma_2}\right)\left(\rho_{e_1e_1} + \rho_{e_2e_2}\right) - \frac{1}{2}(r_1 + r_2 + \Gamma_1 + \Gamma_2 + 2\Gamma_D)\rho_{e_1e_2} - i\Delta\rho_{e_1e_2}. \tag{12c}$$

Consider first the case of $p = 0 = P$ in which no steady-state coherences were observed in previous studies.[26,29,33,34,42,47,51] The master equations [Eq. (12)] can be simplified and written in a matrix form as follows:

$$\dot{\boldsymbol{\rho}} = \hat{A}\boldsymbol{\rho}, \tag{13a}$$

$$\boldsymbol{\rho} = [\rho_{gg}, \rho_{e_1e_1}, \rho_{e_2e_2}, \rho^R_{e_1e_2}, \rho^I_{e_1e_2}]^T, \tag{13b}$$

$$\hat{A} = \begin{bmatrix} -(r_1+r_2) & r_1+\Gamma_1 & r_2+\Gamma_2 & 0 & 0 \\ r_1 & -(r_1+\Gamma_1) & 0 & 0 & 0 \\ r_2 & 0 & -(r_2+\Gamma_2) & 0 & 0 \\ 0 & 0 & 0 & -\frac{1}{2}(r_1+r_2+\Gamma_1+\Gamma_2)-\Gamma_D & \Delta \\ 0 & 0 & 0 & -\Delta & -\frac{1}{2}(r_1+r_2+\Gamma_1+\Gamma_2)-\Gamma_D \end{bmatrix}, \tag{13c}$$

where $\rho^R_{e_1e_2} = \mathrm{Re}[\rho_{e_1e_2}]$ and $\rho^I_{e_1e_2} = \mathrm{Im}[\rho_{e_1e_2}]$. Examining Eq. (13c) shows that, in the $p = 0 = P$ case, the coherences and state populations decouple. Therefore, a system with no initial excited state coherences will show no coherences between the excited states at any later time. This is the case for a system with no initial excited state populations, as in the excitation of biomolecules in nature. Hence, if $p = 0 = P$, no steady-state coherences will be observed.

To simplify calculations for nonzero p and P, consider now the case of $r_1 = r_2$ and $p = 1 = P$. Rewriting the simplified Eq. (12) in a matrix form gives

$$\hat{A} = \begin{bmatrix} -2r & r+\Gamma_1 & r+\Gamma_2 & 2(r+\sqrt{\Gamma_1\Gamma_2}) & 0 \\ r & -(r+\Gamma_1) & 0 & -(r+\sqrt{\Gamma_1\Gamma_2}) & 0 \\ r & 0 & -(r+\Gamma_2) & -(r+\sqrt{\Gamma_1\Gamma_2}) & 0 \\ r & -\frac{1}{2}(r+\sqrt{\Gamma_1\Gamma_2}) & -\frac{1}{2}(r+\sqrt{\Gamma_1\Gamma_2}) & -(r+\frac{1}{2}(\Gamma_1+\Gamma_2))-\Gamma_D & \Delta \\ 0 & 0 & 0 & -\Delta & -(r+\frac{1}{2}(\Gamma_1+\Gamma_2))-\Gamma_D \end{bmatrix}. \tag{14}$$

In this case, there is a coupling between populations and coherences.

Expressing the master equations in a matrix form as in Eq. (13) shows that the steady states of the system are given by the null space of the matrix $\hat{A}$ in Eq. (14). Calculating the steady state in this way gives

$$\lim_{t\to\infty}\rho^R_{1,2}(t) = \frac{\sqrt{\Gamma_1\Gamma_2}-r}{r+\frac{1}{2}(\Gamma_1+\Gamma_2)} \times \left(\frac{r+\frac{1}{2}(\Gamma_1+\Gamma_2)+\Gamma_D}{(r+\frac{1}{2}(\Gamma_1+\Gamma_2)+\Gamma_D)(\delta+\Gamma_D)+\Delta^2}\right)\delta \lim_{t\to\infty}\rho_e(t), \tag{15a}$$

$$\lim_{t\to\infty}\rho^I_{1,2}(t) = -\frac{\Delta}{r+\frac{1}{2}(\Gamma_1+\Gamma_2)}\lim_{t\to\infty}\rho^R_{1,2}(t), \tag{15b}$$

where $\rho_e = \rho_{e_1,e_1} + \rho_{e_2,e_2}$ is the total population of the excited state manifold and $\delta = \frac{1}{2}(\sqrt{\Gamma_1}-\sqrt{\Gamma_2})^2$ measures the difference in decay rates. It is clear that, in this case of equal pumping rates and $p = 1 = P$, coherences vanish when $\Gamma_1 = \Gamma_2$. This same calculation can be repeated for arbitrary values of r_1 and r_2. While the resulting expression is extremely unwieldy, it can be shown that steady-state coherences vanish when $r_1/\Gamma_1 = r_2/\Gamma_2$. In the one-bath case, the incoherent pumping and spontaneous emission rates are related by fluctuation dissipation relations to the occupation number of the field at ω_0, $\bar{n} = r_i/\gamma_i$. This guarantees that no steady-state coherences can be observed under excitation by a single continuous-mode thermal bath. Rather, it is the competition between the two baths with "incompatible" rates that leads to the steady-state coherences. In this sense, the steady-state coherences are manifestations of a nonequilibrium steady state arising due to the system behaving as a transport medium between two thermal baths of different temperatures.

III. TWO-STATE TWO-MODE MODEL

The 2S2M model[3,22] is a widely used minimal representation of retinal in rhodopsin that includes the key electronic, torsional, and vibronic degrees of freedom and a conical intersection between the ground and first excited states of retinal. This model captures the ultrafast bath-induced relaxation of retinal and reproduces the observed quantum yield and transient absorption spectrum on the picosecond time scales.[52,61]

The system Hamiltonian, $\hat{H}_S$, describes two collective modes, one high frequency stretch x and one low frequency tuning mode $\phi \in [-\pi/2, 3\pi/2]$, describing the photoisomerization dynamics. The 11-*cis*-isomer corresponds to $\phi \in [-\pi/2, \pi/2]$, while the all-*trans*-isomer corresponds to $\phi \in [\pi/2, 3\pi/2]$. The Hamiltonian, $\hat{H}_S$, is given by

$$\hat{H}_S = \sum_{n,n'}\Big[\Big(\hat{T} + E_n + (-1)^n\frac{1}{2}\tilde{V}_n(1-\cos\phi) + \frac{1}{2}\omega x^2 + \kappa x\delta_{n,1}\Big)\delta_{n,n'} + \lambda x(1-\delta_{n,n'})\Big]|n\rangle\langle n'|, \tag{16}$$

where $\hat{T}$ is the nuclear kinetic energy, $|n = 0, 1\rangle$ are the ground and first excited diabatic electronic states, E_n are the energy shifts of the electronic states ($E_0 = 0$), and κ, ω, λ, and $\tilde{V}_n$ are the 2S2M model parameters calculated in Refs. 3 and 22. This Hamiltonian produces a conical intersection at $x = 0$ and $\phi = \pi/2$ that has been shown to lead to highly nonadiabatic dynamics and rapid nonradiative relaxation from the excited electronic state.[21] The adiabatic potential energy surface corresponding to this model Hamiltonian are shown in Fig. 2.

We consider the dynamics of retinal excited by sunlight, which can be modeled by a broadband field of blackbody radiation at a temperature of $T_{rad} = 5700$ K. For simplicity, in this study, we neglect the attenuation of incident light by the eye.[39] However, these effects can be included phenomenologically in the PSBR formalism by introducing a constant C that modifies the mean photon number. This introduces an effective photon occupation $\tilde{n}(\omega) = C\bar{n}(\omega)$ that can be used in place of $\bar{n}(\omega)$. In this paper, we consider a protein bath at room temperature $T_{ph} = 298$ K coupled to each bath mode $\alpha = x$, ϕ with an Ohmic spectral density $J_\alpha(\omega) = \eta_\alpha \omega e^{-\omega/\omega_{CC,\alpha}}$, coupling parameters ($\eta_\alpha$), and a cutoff frequency ($\omega_{CC,\alpha}$) derived in Refs. 21 and 61. These are given by $\eta_x = 0.025$, $\omega_{CC,x} = 0.19$ eV, $\eta_\phi = 0.05$, and $\omega_{CC,\phi} = 0.035$ eV. The system mode operators that couple to the phonon bath in Eq. (7) are given by $\hat{A}_\phi = |\psi_1\rangle\langle\psi_1|(1 - \cos\phi)$ and $\hat{A}_x = |\psi_1\rangle\langle\psi_1|x$,[21,61] where $|\psi_1\rangle$ is the excited electronic state. Further details regarding the system and bath parameters are given in Refs. 21 and 61.

The Markovian approximation in standard Redfield theory, used here, is valid as long as the dynamical time scales of interest in the system are longer than the correlation time of the bath, $\tau_C = 1/\omega_{CC}$. This is well satisfied for the system examined here which shows correlation times $\tau_C \sim 1$–10 fs, while the relevant dynamical processes in the system occur several orders of magnitude slower ~0.1–1 ps. Moreover, perturbative Redfield theories are known to be valid when the parameter $\eta_{\text{Redfield}} := \max\{k_B T\eta/\omega_{CC}^2, \eta/\pi\omega_{CC}\}$ is less than or on the order of 1.[53] The baths considered in this study are within this domain of applicability. The room temperature bath does not significantly excite higher lying states in the 2S2M model. To simplify modeling, we therefore consider a system that is initially in the lowest energy 2S2M state before the turn-on of the incoherent light.

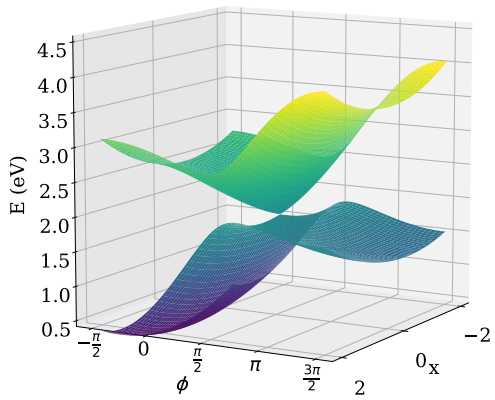

FIG. 2. Adiabatic potential energy surfaces of the two-state two-mode model[22] of retinal described by Eq. (16). The coordinates x and $\phi \in [-\pi/2, 3\pi/2]$ describe collective modes of retinal with the 11-*cis*-isomer corresponding to the region $\phi \in [-\pi/2, \pi/2]$ and the all-*trans*-isomer to $\phi \in [\pi/2, 3\pi/2]$. The adiabatic curves display a conical intersection at $x = 0$ and $\phi = \pi/2$.

For retinal in rhodopsin, nonradiative decay processes coupled to the local protein phonon environment occur several orders of magnitude faster than fluorescence decay between the bright and ground states.[3,22] As a result, retinal decays to the product state manifold through a cascade of intermediate dark states that are not coupled to the ground state by the light field.[51] Hence, the light field drives the initial population of the bright states, and nonradiative (rather than fluorescent) decay will dictate the relaxation from the bright state. Consequently, it is the interplay between the time-dependent initial excitation and the time-independent nonradiative dissipation that is responsible for the emergence of the nonequilibrium steady state. Qualitatively, this is due to two sources of noise-induced coherences: incoherent light and the thermal phonon protein environment.

It is significant to note at the outset a number of time scales. In the human eye, blinking, which turns on the light incident on the retina, takes ~100 ms. Reported time scales for subsequent molecular processes[62] show pulsed laser-induced conversion of 11-*cis*-retinal to all-*trans* retinal in less than 200 fs, with concomitant transition from rhodopsin to photorhodopsin. The latter relaxes within a few ps to bathorhodopsin which decays to lumirhodopsin on a 100 ns time scale. Subsequent steps lead to ejection of the retinal from metarhodopsin formed on ms time scales and signaling on ms and longer time scales. This being the case, turn-on times of the light are on the same order of magnitude as the ejection of the retinal chromophore. Ideally then, we should consider time scales that include slow turn-on of incoherent excitation through the subsequent formation of a steady state that includes formation of metarhodopsin. However, since steps until ejection of retinal from metarhodopsin all occur with retinal bound to an opsin moiety, we focus on retinal behavior with slowly turned on incoherent light in a model environment in which the dynamics of the environment are assumed contained. Computations are restricted to turn-on times less than 10 ps and dynamics of either 3 ps or three times the turn-on time, whichever is larger. In this 2S2M model, an overall steady state, where *cis* and *trans* populations are constant in time, is known to be reached on a time scale of 10^{-5} s.[63] However, a pseudosteady nonequilibrium state, here viewed as the NESS, is defined as the time where the quantum yield is constant. As shown below, this is reached in 1 ps. Extrapolating the results of this study to natural turn-on times of 100 ms implies extrapolation of 11 orders of magnitude. With this in mind, however, the results obtained below will be seen to be both enlightening and meaningful. Future work will examine more complex environmental dynamics.

IV. CHARACTERIZING RETINAL PHOTOISOMERIZATION DYNAMICS

A. Populations, coherence ratio, and quantum yield

To examine aspects of the turn-on of noise-induced coherences in retinal, the master equation [Eq. (2)] is numerically integrated under the approximations described above. The dependence of the coherences on the turn-on time of the light is examined

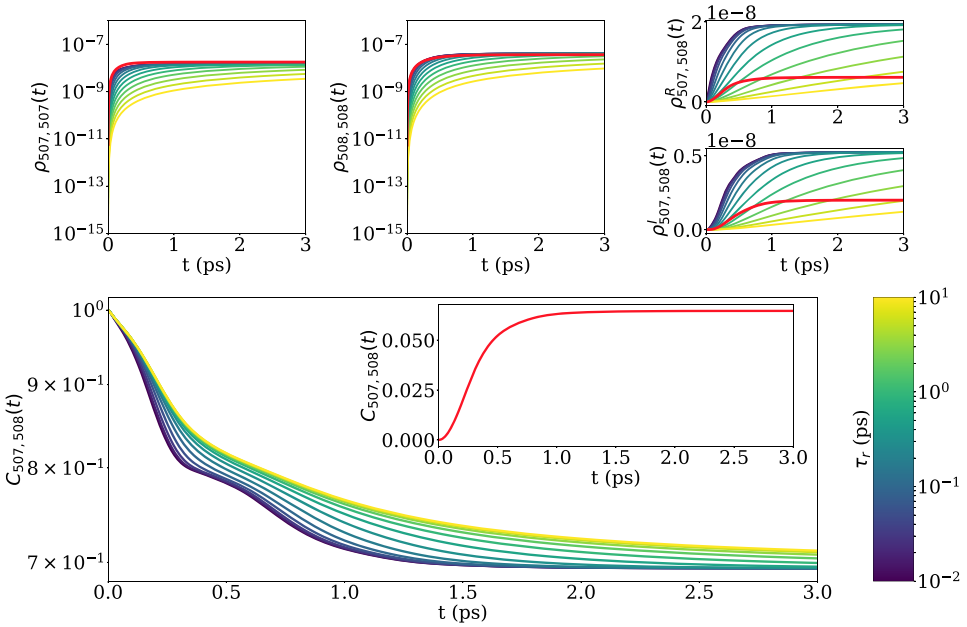

FIG. 3. The density matrix elements (top) and coherence ratio (bottom) corresponding to a pair of nearly degenerate bright states (|507⟩ and |508⟩ with $\omega_{507,508}$ = 2.39 cm^{-1}) under a range of light-field turn-on times (yellow-blue curves). These are contrasted with the case where light-induced coherences are artificially suppressed (red curves) by setting $p_{ij} = \delta_{ij}$ in Eq. (4).

and seen to provide considerable insight into the role of light-induced coherences. To display the results, the populations of and coherences between several representative pairs of energy eigenstates are considered with varying turn-on times and with light-induced coherences either included or artificially suppressed. As mentioned above, the latter results expose the interplay between the time-dependent incoherent driving and the time-independent dissipation. Light-induced coherences between nearly degenerate and energetically distant eigenstates were found to respond differently to the slow turn-on of light.[28] Therefore, one pair of bright states (i.e., states excited by the incident light) is considered in each of these limits. Furthermore, the vibrational environment is expected to play a more significant role for states further along the bath-induced relaxation cascade, suggesting that intermediate and product states may respond differently to the time-varying driving field. Hence, one pair of intermediate states and one pair of product states are examined. Figures 3–6, showing these results, are discussed below.

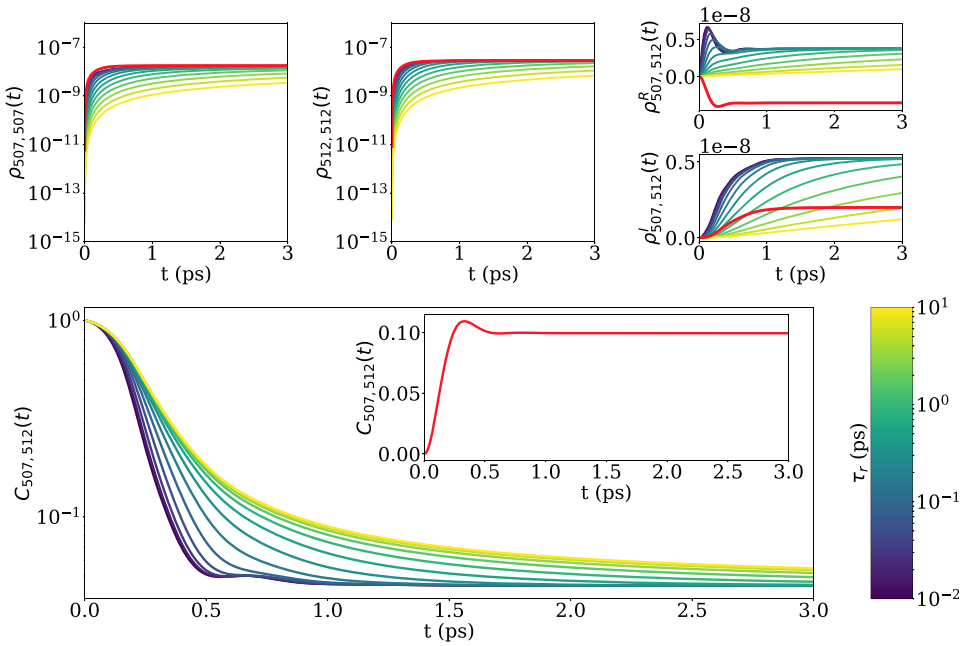

FIG. 4. The density matrix elements (top) and coherence ratio (bottom) corresponding to a pair of energetically distant bright states (|507⟩ and |512⟩ with $\omega_{507,512}$ = 74.2 cm^{-1}) under a range of light-field turn-on times (yellow-blue curves). These are contrasted with the case where noise-induced coherences are artificially suppressed (red) by setting $p_{ij} = \delta_{ij}$ in Eq. (4).

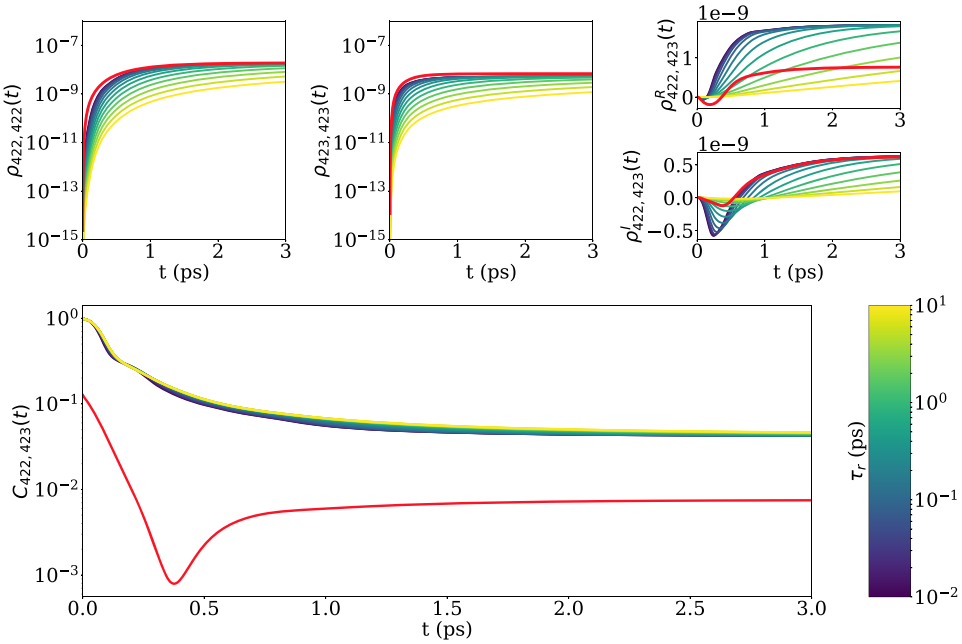

FIG. 5. The density matrix elements (top) and coherence ratio (bottom) corresponding to a pair of intermediate dark states (|422⟩ and |423⟩ with $\omega_{422,423}$ = 14.4 cm^{-1}) under a range of light-field turn-on times (yellow-blue curves). These are contrasted with the case where noise-induced coherences are artificially suppressed (red) by setting $p_{ij} = \delta_{ij}$ in Eq. (4). Note the difference in ordinate scales from the bright state figures.

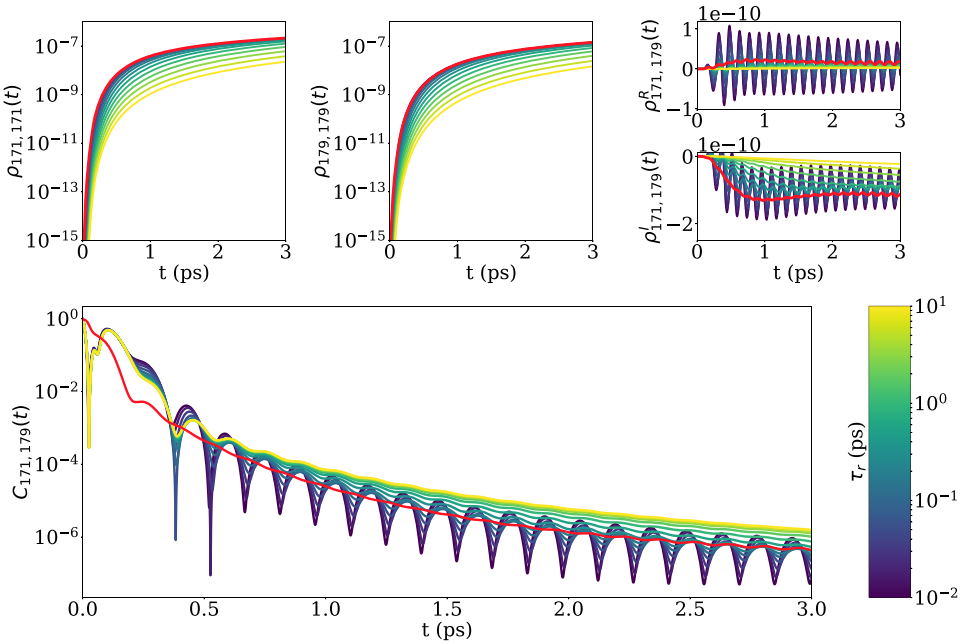

FIG. 6. The density matrix elements (top) and coherence ratio (bottom) corresponding to a pair of dark product states (|171⟩ and |179⟩ with $\omega_{507,508}$ = 553.0 cm^{-1}) under a range of light-field turn-on times (yellow to blue curves). These are contrasted with the case where noise-induced coherences are artificially suppressed (red) by setting $p_{ij} = \delta_{ij}$ in Eq. (4). Note the difference in ordinate scales from prior figures.

Amongst these results, we also show the following coherence ratio:

$$C_{ij}(t) := \frac{|\rho_{ij}(t)|^2}{\rho_{ii}(t)\rho_{jj}(t)}. \tag{17}$$

This measure has been previously used to characterize noise-induced coherences in simple systems and provides a method to compare such coherences between different pairs of states irrespective of their relative populations.[26,42] Throughout, two different sets of results are shown: various colored curves other than red for different turn-on times and a red curve corresponding, for comparison, to the case where light-induced coherences are suppressed [i.e., $p_{ij} = \delta_{ij}$ in Eq. (4)]. The red $p_{ij} = \delta_{ij}$ curve assumes the sudden turn of the radiation and exposes the coherences due to the system

interacting with the incoherent phonon environment. It is particularly relevant at longer times, when it is time independent, in providing the contribution to the coherences solely due to the interaction with the incoherent phonon bath, with no initial light-induced coherence.

In addition, we consider the overall effect of coherences and turn-on times on the isomerization quantum yield. Specifically, we define $Y_1(t)$, the time-dependent quantum yield, as the fraction of product state population in the all-*trans* state. For retinal in the 2S2M model, the yield is given by[52]

$$Y_1(t) = \frac{\langle \hat{P}^{(1)}_{trans}(t)\rangle}{\langle \hat{P}^{(0)}_{cis}(t)\rangle + \langle \hat{P}^{(1)}_{trans}(t)\rangle}, \tag{18a}$$

$$\hat{P}^{(0)}_{cis} = \Theta(\pi/2 - |\phi|)|\psi_0\rangle\langle\psi_0|, \tag{18b}$$

$$\hat{P}^{(1)}_{trans} = \Theta(|\phi| - \pi/2)|\psi_1\rangle\langle\psi_1|, \tag{18c}$$

where the *cis* and *trans* projectors are given by Eqs. (18b) and (18c). They divide the isomerization range of the torsional degree of freedom into *cis* ($\phi \in [-\pi/2, \pi/2]$) and *trans* ($\phi \in [\pi/2, 2\pi/2]$) regions. These projectors, $|\psi_n\rangle\langle\psi_n|$, project onto the ground $|\psi_0\rangle$ and excited $|\psi_1\rangle$ diabatic electronic states, and $\Theta(x)$ is the Heaviside step function. The averages in Eqs. (18a)–(18c) are over the ensemble generated by the master equation dynamics. The calculated time-dependent quantum yield is discussed below.

B. Dynamical evolution

First, consider the dynamics and coherences between different pairs of states. Results are provided in Figs. 3–6. They are all constructed in the following way. The four figures in the top row show populations of the two levels in each pair as well as the real and imaginary parts of the coherences between them. The lower row provides an analysis of the coherences renormalized to account for the population of the corresponding eigenstates, i.e., they show $C_{ij}(t)$. The latter is discussed in Sec. IV C.

Figures 3 and 4 show populations and coherences for two different pairs of bright states, the closely spaced $|507\rangle$, $|508\rangle$ and the more widely spaced $|507\rangle$, $|512\rangle$ pairs. The former are energetically separated by $\omega_{507,508} = 2.39\ \text{cm}^{-1}$ and the latter by $\omega_{507,512} = 74.2\ \text{cm}^{-1}$. The upper set of panels show the populations of the states and the coherences between them as a function of time and as a function of turn-on time. Populations for different turn-on times are seen to rise over time and begin to converge at t ~ 3 ps, where they still differ by over an order of magnitude. Distinct amongst these curves is the red curve, i.e., sudden turn-on of the light in the absence of light-induced coherences. Of relevance at long times, this curve is seen to be an upper bound to the populations induced in the presence of light-induced coherences. That is, the light-induced coherences serve to enhance population decay, manifest here as suppressed excited state populations.

The upper right-hand panels display the real and imaginary parts of the coherences $\rho^R_{507,508}(t)$ $\rho^I_{507,508}(t)$, $\rho^R_{507,512}(t)$, and $\rho^I_{507,512}(t)$; they are seen to rise increasingly slowly as the turn-on time of the light is increased from 10^{-2} ps and 1 ps. (Natural turn-on times are orders of magnitude longer.) Any oscillatory contribution, e.g., in the (507, 512) case, reminiscent of previously observed oscillations for fast pulses, appears for only the shortest of turn-on times. As the turn-on time exceeds the period of 0.5 ps, these oscillatory coherences disappear entirely. Examining the coherences for longer times shows that $\rho^R_{507,512}$ approaches 3.6×10^{-9}, equivalent in magnitude to the populations.

It is crucial to appreciate that all the coherence curves (other than the red line) will converge at long times to the blue curve, i.e., to a long-time nonequilibrium steady state. This state manifests effects due to both the initially created light-induced coherences and the coherences induced by the system interacting with the environment. A comparison of the role of the former is afforded by the light-induced coherence-free red curve. At the longer times when these curves are useful for comparison, they are seen to be significantly different in magnitude from the curves of various other colors. Hence, the interplay of the coherences induced by the incoherent light and that induced by the system-phonon interaction are seen to affect both the state populations and the associated coherences. Furthermore, it is important to emphasize that these (Fano) coherences induced by the incoherent light (for $p_{ij} \neq 0$ for $i \neq j$) are significantly different from those resulting from irradiation with coherent light, i.e., that seen with laser excitation,[23,26,28] as discussed in Sec. II B.

Note that the character of the coherences is hidden by the fact that slow turn-on produces small populations and hence small coherences. As a consequence, an analysis in terms of C_{ij} [Eq. (17)] in Secs. IV C and V will prove enlightening. In addition, Figs. 3 and 4 refer to the bright states excited by the incident light. As time progresses, this excitation and coherence is transferred to lower energy states as the system relaxes. This is also discussed below.

C. Coherences

The *character* of the coherences prepared upon excitation, and subsequently as the system relaxes to the NESS, is of great interest. Consider first the bright states. As shown in the lower panels of Figs. 3 and 4, these states are, remarkably, initially excited into pure coherent superpositions [$C_{ij}(0) = 1$], despite the incoherent light source. The initial preparation is typical of the development of Fano coherences when $p_{ij} = 1$.[28] They then subsequently decay in several hundred femtoseconds as the growth of the populations outpaces the growth of the coherences.

As a consequence, the coherences decay on the same time scale as the turn-on time. What is also evident is the loss of $C_{ij}(t)$ short time oscillations as the turn-on time increases. That is, the blue curves corresponding to fast $\tau_r \sim 10^{-2}$ ps turn-on show $C_{ij}(t)$ oscillations at times less than 1 ps, which disappear as the turn-on times become longer. These are essentially oscillatory dynamics induced by the rapid turn-on of the incoherent light. They are, of course, irrelevant in a biological context where turn-on times are orders of magnitude longer.

By contrast, when light induced coherences are artificially suppressed, as shown in the red curve in the inset panel, the system is first driven into an incoherent mixture of energy eigenstates [$C_{ij}(0) = 0$] but then begins to develop, after ~100 fs, coherences induced by the phonon vacuum (i.e., due to the spontaneous emission of phonons into the protein environment). After 1 ps, these coherences are constant and independent of turn-on times. They are equivalent to the well understood vacuum-induced coherences that occur

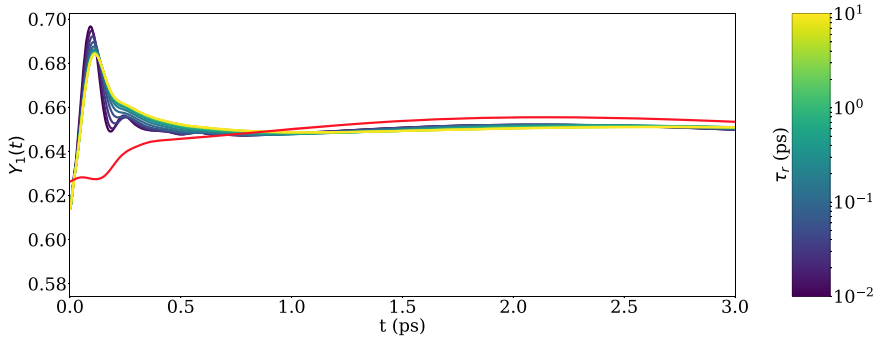

FIG. 7. Time-dependent quantum yield with varying turn-on times τ_r (yellow-blue curves). These are contrasted with the case where light-induced coherences are artificially suppressed (red curve) by setting $\rho_{ij} = \delta_{ij}$ in Eq. (4).

through fluorescent decay,[44,57] here with a bosonic phonon bath replacing the electromagnetic bath.

After initial excitation to the bright states, retinal undergoes nonradiative relaxation through a series of intermediate states before reaching the products state manifold. Consider first the populations and coherences of these states, the upper row in Figs. 5 and 6. The coherent dynamics between a pair of close-lying intermediate states $|422\rangle$ and $|423\rangle$ are shown in Fig. 5. Since the intermediate states are populated by nonradiative decay, attempting to categorize them as oscillatory or quasistationary, as was previously the case for radiative excitation, does not apply, and the dynamics can be more complicated. This is seen, for example, in Fig. 5 where the τ dependence of the coherences is neither oscillatory-like nor quasi-stationary-like coherences. Furthermore, the coherences in Fig. 5 are an order of magnitude smaller than those in Figs. 3 and 4. Surprisingly, the short-time dynamics do appear qualitatively different for faster and slower turn-ons, with the short time coherence features vanishing under slower turn-on.

Consider now the dynamics in the product state manifold, shown in the upper row of Fig. 6 for a pair of product states. Focusing first on the short-time dynamics, the same indirect slow turn-on and alignment parameter effects described for dynamics on the intermediate state manifold apply to product-state coherent dynamics here as well. With increasing turn-on time, short time features such as oscillations decrease in magnitude and eventually disappear. Furthermore, coherences show a qualitative dependence on the p alignment parameter, suggesting that dynamics on the product state are influenced by the light-induced coherences on the bright state through interference effects in the nonradiative relaxation cascade. The long-time dynamics show that, despite the loss in magnitude of the short-time oscillations in coherences, the coherences increase with time along with the populations. This suggests that, even in the slow turn-on limit, a coherent superposition of product energy eigenstates is produced. However, the magnitude of these coherences is very small. This is driven by the rhodopsin phonon bath and complements a previous study examining the nonradiative cascade from an incoherent mixture of bright states[52] into a partition of local *cis* and *trans* states. This study considered only secular excitation, where the light field generates no coherence.

D. The quantum yield

The dependence of the quantum yield on the light turn-on time (Fig. 7) adds considerable insight into the approach of the system to the steady state. This quantity reflects the contributions of all of the density matrix elements and hence captures cumulative effects that can manifest through small changes in many of the matrix elements that may not appear when they are examined separately.

Note first that the quantum yield becomes relatively constant at 1 ps, establishing an NESS. In contrast to the behavior of individual matrix elements, the quantum yield shows some transient features that disappear in the slow turn-on and others that remain robust to turn-on times that are much slower than the times at which these features appear. The ~100 fs *oscillatory* features of the quantum yield correspond to the influence of oscillatory light-induced coherences in the bright state (as can be seen by their disappearance in both the slow turn-on limit and when light-induced coherences are suppressed). As these transient features disappear from the density matrix dynamics (see Figs. 3 and 4), they no longer influence the quantum yield.

V. DISCUSSION OF NUMERICAL RESULTS

We now consider the physical interpretation of several puzzling observations seen in the numerical simulation of retinal. First, we turn our attention to the apparent slow turn-on of phonon-induced coherence seen in Figs. 5 and 6. This can be easily understood by considering the source terms that drive the density matrix elements of the dark state subspace. These terms take a form $\mathcal{R}_{ij,kl}\rho_{ij}$, where $|i\rangle$ and $|j\rangle$ are bright states and $|k\rangle$ and $|l\rangle$ are dark states. While the relaxation tensor for these phonon-driven processes is independent of the slow turn-on of light, the bright state density matrix elements depend very strongly on it. As a result, this creates an effective slow turn-on that is apparent even in states that are not directly populated by light. Interestingly, although the alignment parameter p refers only to the transition dipole moments that drive light-induced processes and has no direct effect on phonon bath coupling, different values of p were seen (e.g., the red curves in the upper panels of Fig. 5) to produce qualitatively different coherences in the intermediate states. This difference in dynamics suggests that different coherent superpositions of intermediate states are occupied for different values of p, indicating that the light-induced coherences in the bright state change the intermediate states through which the nonradiative relaxation cascades and therefore can alter the steady state of the system in the product manifold.

Consider now the analysis of the coherences in the lower panel in Figs. 5 and 6. Note that intermediate states with suppressed light-induced coherences (Fig. 5) display some initial coherence,

while product states (Fig. 6) are initially prepared in nearly coherent superpositions, i.e., $C_{ij} \sim 1$. This increasing coherence arises due to the accumulation of phonon-induced coherences with each phonon coupled transition. In particular, before significant dephasing occurs, the vibrational environment induces transitions from one pure state to another. So, for systems with light-induced coherences, the initially prepared bright-state superposition will decay into coherent superpositions at all points along the dissipative cascade, giving $C_{ij}(0) = 1$ among all states. By contrast, when light-induced coherences are suppressed, each eigenstate in the initially excited incoherent bright state mixture will generate a coherent superposition in the intermediate state manifold, each of which subsequently generates coherent superpositions in the product manifold, accumulating coherence in each transition. This is evident in the magnitude of C_{ij} (red curve) in going from Fig. 4 to Fig. 6.

As discussed in Sec. II B, the initial excitations prepared at $t = 0$ are fully coherent. Since the phase of the incident light shows no fluctuation in the first instant on which it is incident on the system, it is indistinguishable from a coherent source. Moreover, the system is driven into the same superposition, determined by the transition dipole moments, for all turn-on times. These initial coherences influence the nonradiative decay out of the bright states through the interference and coherence transfer processes outlined in Sec. II C and can lead to dynamical features at very short times that do not depend on the turn-on time of incident light (e.g., the immediate drop and re-emerging peak of $C_{171,179}$ in Fig. 6). However, the rate at which this excitation occurs is clearly dependent on the incident light-intensity and is therefore sensitive to the turn-on time. Consequently, the slow turn-on of light significantly modifies the subsequent dynamics after the decay of the initial superposition (e.g., the loss of $C_{171,179}$ oscillations in Fig. 6).

Surprisingly, the loss of fast light-induced dynamics is not only seen in the bright states directly excited by the incoherent light. The dynamics of dark states that are not directly accessible by photoexcitation show an unexpected dependence on the turn-on time of the light (Figs. 5 and 6). The appearance of slow turn-on effects in the dark state manifold is at first counterintuitive as their population is driven by time-independent nonradiative processes. However, as discussed in Sec. II C, vibration-induced relaxation is sensitive to light-induced coherences. In particular, simultaneous nonradiative decay can lead to the transfer of light-induced coherence to lower-lying dark states. For example, this coherence transfer mechanism generates the dramatic oscillations in Fig. 6 in the presence of light-induced coherences. When light-induced coherences are suppressed, this oscillatory behavior vanishes, indicating that it arises due to the transfer of light-induced coherences rather than being directly generated by the protein environment. As the turn-on time of the light increases, these oscillations are suppressed as the bright excited states no longer display oscillatory coherence.

By contrast, the transient quantum yield *enhancement* appearing at 100 fs, while small, is robust at all turn-on times studied, including those several orders of magnitude slower than 100 fs. This feature is notably absent when light-induced coherences are suppressed (red curve in Fig. 7) and hence is a consequence of the initially prepared bright state superposition. Although this effect is weak in retinal isomerization, its manifestation in realistic fields indicates that coherent effects can survive under biological conditions, suggesting that they may play a larger role in other biomolecules. The decay of coherent superpositions initially prepared in the bright-state is different from that of incoherent mixtures, due to interference and coherence transfer in the nonradiative decay process. This can be seen in the different short time (~100 fs) density matrix dynamics of all the states examined in the absence of light-induced coherences (red traces in Figs. 3–6). Significantly then, the turn-on time independence of the transient quantum yield enhancement therefore reflects the τ_r independence of the initially generated coherent superposition and consequently is expected to be robust for turn-on times longer than those studied, including realistic turn-on times on the order of milliseconds.

VI. CONCLUSION

In this study, we have provided an account for the coherences that can arise in a light-driven biomolecular system in the Markovian Redfield limit, describing their physical origin and the conditions under which they occur. We then illustrate the role of these coherences in a 2S2M model of retinal photoisomerization, revealing a loss of noise-induced coherent dynamical features in the slow turn-on limit. However, due to the interplay between the two baths, several coherent features survive the slow turn-on of light. First, the initial coherent superposition excited from the ground state is shown to be independent of the turn-on time and is in fact, identical to laser excitation. Although the slow turn-on then suppresses coherence oscillations, a coherent nonequilibrium steady-state emerges as a result of *transport-induced coherences*. This form of coherence arises due to the continuous dissipation of energy from the incident-light into the phonon environment and leads to the breaking of fluctuation-dissipation constraints on the quantum rate constants. Interestingly, these coherences are extremely different from those resulting from laser excitation.

These results identify robust coherences that can arise in a model biomolecule under realistic photoexcitation conditions and describe the physical mechanisms that generate them. While traditional laser-induced oscillatory coherences may not arise in nature, the coherent effects seen in this paper suggest that a very different type of quantum effect may be seen in biological systems. This motivates further studies that probe the dynamics of retinal into longer biochemical time scales, highlighting the need for new methods to efficiently estimate the quantum dynamics of complex systems. Furthermore, while the coherent effects seen in retinal were relatively small, producing an increase of ~5% in the quantum yield, they indicate that coherent effects can occur under realistic conditions. Other biomolecular systems, such as photosynthetic light harvesting systems, may display more significant quantum enhancements. Finally, the observation of these steady-state coherences raises questions about the nature of the NESS. In particular, it remains to be seen whether these steady-state coherences enhance the steady-state function in realistic systems.

ACKNOWLEDGMENTS

Support from the U.S. Air Force Office of Scientific Research (AFOSR) under Contract No. FA9550-17-1-0310 is gratefully acknowledged.

APPENDIX: SEMICLASSICAL LIGHT-INDUCED COHERENCES

Here, we provide a description of the phase of excitations generated by semiclassical light and derive Eq. (6). The light is taken to be weak and therefore in the regime of linear optics. Excitation by natural incoherent light is known to be well treated by this level of theory. Furthermore, since we consider a semiclassical light field, first-order time-dependent perturbation theory in the wavefunction can be used to treat the resultant molecular dynamics.

Consider a molecular system with energy eigenbasis $\{|i\rangle\}$ and energies $\{\epsilon_i\}$ that is driven by the electromagnetic field given by Eq. (5). Under the dipole approximation, the interaction between the system and light field is given by

$$\hat{V}(t) = \sum_{i \neq j} \mu_{ij} E^+(t) |i\rangle\langle j|, \tag{A1}$$

where μ_{ij} is the transition dipole moment between energy eigenstates $|i\rangle$ and $|j\rangle$ and is taken to be real for simplicity.

The dynamics of the molecular system driven by this field is given by

$$c_i(t) := \langle i|\psi(t) \approx c_i(0) e^{-i\epsilon_i t/\hbar} + \int_0^t dt' c_i^{(1)}(t;t'), \tag{A2a}$$

$$c_i^{(1)}(t;t') = \langle i| e^{-\frac{i}{\hbar}\hat{H}(t-t')} \hat{V}(t') e^{-\frac{i}{\hbar}\hat{H}t'} |\psi(t)\rangle, \tag{A2b}$$

where $|\psi(t)\rangle = \sum_i c_i(t)|i\rangle$ and $c^{(1)}(t;t')$ gives the contribution of the system-field interaction, occurring at time t', to the coefficient c_i at time t.

Equation (A2b) can now be used to find the relative phase between two states excited by $E^+(t)$. To do this, consider a system initially in its ground state $|g\rangle = |0\rangle$ with energy $\epsilon_0 = 0$ [i.e., $c_g(0) = 1$]. The relative phase between two states is given by $\Delta\phi_{ij}(t) = \log(c_i(t)c_j^*(t)/|c_i(t)c_j^*(t)|)$. Using Eq. (A2),

$$c_i(t)c_j^*(t) = \int_0^t dt_i \int_0^t dt_j c_i^{(1)}(t;t_i) c_j^{(1)*}(t;t_j) \tag{A3}$$

$$= \int_0^t dt_i \int_0^t dt_j A(t_i) A(t_j) \mu_{gi}\mu_{gj} \times e^{-i\left[\phi(t_j)-\phi(t_i)+\frac{(\epsilon_j-\epsilon_i)}{\hbar}(t-t_j)-\frac{\epsilon_i}{\hbar}(t_j-t_i)\right]}, \tag{A4}$$

where the integrand gives the contribution of an excitation to state i at time t_i and an excitation to state j at time t_j to the dynamics at time t. The relative phase of this contribution then gives Eq. (6).

We note that this time domain treatment differs from the typical frequency domain picture. In the latter, Eq. (5) is Fourier transformed to give frequency-dependent amplitudes and phases

$$E^+(t) = \int d\omega \tilde{A}(\omega) e^{-i\phi(\omega)} e^{-i\omega t}, \tag{A5}$$

where $\tilde{A}(\omega)$ and $\phi(\omega)$ are real valued and define the amplitude and phase of the component of $E^+(t)$ with frequency ω, respectively.

This Fourier representation of semiclassical light is convenient since it reveals resonance conditions that relate transitions between two states i and j to a single frequency $\omega_{ij} = |\epsilon_j - \epsilon_i|/\hbar$. Consider the contribution of each frequency component $E^+_\omega(t) = \tilde{A}(\omega) e^{-i\phi(\omega)} e^{-i\omega t}$ separately by substitution into Eq. (A2). This shows that excitation from state $|i\rangle$ to state $|j\rangle$ is driven only by the field component with resonant frequency ω_{ij}. This arises since excitation contributions at all times t' originating from state $|j\rangle$ [i.e., $c_j^{(1)}(t;t')$ assuming $c_j(0) = 1$] are always in phase. For any other frequency components, these contributions will not be in phase and will destructively interfere, leading to no excitation.

If we now consider excitation from the ground state $|g\rangle$ as we did in Eq. (A3), we see that the phase of the wavefunction on state $|i\rangle$ does not depend on the excitation time t_i and is given by $\phi_i(t;t_i) = \phi(t) = \omega_{gi}t + \phi(\omega_{gi})$. The relative phase between states $|i\rangle$ and $|j\rangle$ is then also independent of the excitation times and is given by the more familiar expression

$$\Delta\phi_{ij}(t;t_1,t_2) = \omega_{ij}t + \phi(\omega_{gi}) - \phi(\omega_{gj}). \tag{A6}$$

While this expression also depends on the phase of the light field through $\phi(\omega)$, it considers the phase at a given frequency and not at a given time. The two results are equivalent but arise as a result of the difference in the field descriptions in Eqs. (5) and (A5).

REFERENCES

[1] R. E. Blankenship, *Molecular Mechanisms of Photosynthesis* (John Wiley & Sons, New York, NY, 2013), oCLC: 904814272.
[2] F. Rieke and D. A. Baylor, Rev. Mod. Phys. **70**, 1027 (1998).
[3] S. Hahn and G. Stock, Chem. Phys. **259**, 297 (2000).
[4] N. Lambert, Y.-N. Chen, Y.-C. Cheng, C.-M. Li, G.-Y. Chen, and F. Nori, Nat. Phys. **9**, 10 (2013).
[5] S. C. Flores and V. S. Batista, J. Phys. Chem. B **108**, 6745 (2004).
[6] G. R. Fleming, G. S. Schlau-Cohen, K. Amarnath, and J. Zaks, Faraday Discuss. **155**, 27 (2012).
[7] G. D. Scholes, G. R. Fleming, A. Olaya-Castro, and R. van Grondelle, Nat. Chem. **3**, 763 (2011).
[8] A. Ishizaki, T. R. Calhoun, G. S. Schlau-Cohen, and G. R. Fleming, Phys. Chem. Chem. Phys. **12**, 7319 (2010).
[9] Y.-C. Cheng and G. R. Fleming, Annu. Rev. Phys. Chem. **60**, 241 (2009).
[10] G. S. Engel, T. R. Calhoun, E. L. Read, T.-K. Ahn, T. Mančal, Y.-C. Cheng, R. E. Blankenship, and G. R. Fleming, Nature **446**, 782 (2007).
[11] Y. Zhang, S. Oh, F. H. Alharbi, G. S. Engel, and S. Kais, Phys. Chem. Chem. Phys. **17**, 5743 (2015).
[12] E. Collini, C. Y. Wong, K. E. Wilk, P. M. G. Curmi, P. Brumer, and G. D. Scholes, Nature **463**, 644 (2010).
[13] J. I. Â. Ogren, A. L. A. Tong, S. C. A. Gordon, A. Chenu, Y. Lu, R. Blankenship, J. Cao, and G. Schlau-Cohen, Chem. Sci. **9**, 3095 (2018).
[14] T. Kondo, A. Pinnola, W. J. Chen, L. Dall'Osto, R. Bassi, and G. S. Schlau-Cohen, Nat. Chem. **9**, 772 (2017).
[15] P. J. M. Johnson, A. Halpin, T. Morizumi, V. I. Prokhorenko, O. P. Ernst, and R. J. D. Miller, Nat. Chem. **7**, 980 (2015).
[16] S. J. Jang and B. Mennucci, Rev. Mod. Phys. **90**, 035003 (2018); e-print arXiv:1804.09711.
[17] D. Montemayor, E. Rivera, and S. J. Jang, J. Phys. Chem. B **122**, 3815 (2018).
[18] S. J. Jang, J. Phys. Chem. Lett. **9**, 6576 (2018).
[19] M. K. Lee, K. B. Bravaya, and D. F. Coker, J. Am. Chem. Soc. **139**, 7803 (2017).
[20] M. K. Lee, P. Huo, and D. F. Coker, Annu. Rev. Phys. Chem. **67**, 639 (2016).
[21] B. Balzer, S. Hahn, and G. Stock, Chem. Phys. Lett. **379**, 351 (2003).
[22] S. Hahn and G. Stock, J. Phys. Chem. B **104**, 1146 (2000).
[23] P. Brumer, J. Phys. Chem. Lett. **9**, 2946 (2018).
[24] X.-P. Jiang and P. Brumer, J. Chem. Phys. **94**, 5833 (1991).
[25] P. Brumer and M. Shapiro, Proc. Natl. Acad. Sci. U. S. A. **109**, 19575 (2012).
[26] T. V. Tscherbul and P. Brumer, Phys. Rev. Lett. **113**, 113601 (2014).
[27] T. Grinev and P. Brumer, J. Chem. Phys. **143**, 244313 (2015).

[28]A. Dodin, T. V. Tscherbul, and P. Brumer, J. Chem. Phys. **145**, 244313 (2016).
[29]T. V. Tscherbul and P. Brumer, J. Chem. Phys. **142**, 104107 (2015).
[30]L. A. Pachon, J. D. Botero, and P. Brumer, J. Phys. B: At., Mol. Opt. Phys. **50**, 184003 (2017).
[31]D. G. S. Agarwal, *Quantum Optics*, Springer Tracts in Modern Physics (Springer Berlin Heidelberg, 1974), Vol. 70, pp. 1–128.
[32]G. S. Agarwal and S. Menon, Phys. Rev. A **63**, 023818 (2001).
[33]K. E. Dorfman, D. V. Voronine, S. Mukamel, and M. O. Scully, Proc. Natl. Acad. Sci. U. S. A. **110**, 2746 (2013).
[34]V. V. Kozlov, Y. Rostovtsev, and M. O. Scully, Phys. Rev. A **74**, 063829 (2006).
[35]B.-Q. Ou, L.-M. Liang, and C.-Z. Li, Opt. Commun. **281**, 4940 (2008).
[36]T. R. Calhoun, N. S. Ginsberg, G. S. Schlau-Cohen, Y.-C. Cheng, M. Ballottari, R. Bassi, and G. R. Fleming, J. Phys. Chem. B **113**, 16291 (2009).
[37]E. Meneghin, A. Volpato, L. Cupellini, L. Bolzonello, S. Jurinovich, V. Mascoli, D. Carbonera, B. Mennucci, and E. Collini, Nat. Commun. **9**, 3160 (2018).
[38]C. Creatore, M. A. Parker, S. Emmott, and A. W. Chin, Phys. Rev. Lett. **111**, 253601 (2013).
[39]K. Hoki and P. Brumer, Procedia Chem. **3**, 122 (2011).
[40]J. Olšina, A. G. Dijkstra, C. Wang, and J. Cao, e-print arXiv:1408.5385 [physics, physics:quant-ph] (2014).
[41]T. Mančal and L. Valkunas, New J. Phys. **12**, 065044 (2010).
[42]A. Dodin, T. V. Tscherbul, and P. Brumer, J. Chem. Phys. **144**, 244108 (2016).
[43]L. A. Pachon and P. Brumer, Phys. Rev. A **87**, 022106 (2013).
[44]S. Menon and G. S. Agarwal, e-print arXiv:quant-ph/9902021 (1999).
[45]G. C. Hegerfeldt and M. B. Plenio, Phys. Rev. A **47**, 2186 (1993).
[46]M. Fleischhauer, C. H. Keitel, M. O. Scully, and C. Su, Opt. Commun. **87**, 109 (1992).
[47]M. O. Scully, K. R. Chapin, K. E. Dorfman, M. B. Kim, and A. Svidzinsky, Proc. Natl. Acad. Sci. U. S. A. **108**, 15097 (2011).
[48]D. Gelbwaser-Klimovsky, W. Niedenzu, P. Brumer, and G. Kurizki, Sci. Rep. **5**, 14413 (2015).
[49]R. Alicki, D. Gelbwaser-Klimovsky, and K. Szczygielski, J. Phys. A: Math. Theor. **49**, 015002 (2016).
[50]J. E. Kim, M. J. Tauber, and R. A. Mathies, Biochemistry **40**, 13774 (2001).
[51]T. V. Tscherbul and P. Brumer, Phys. Chem. Chem. Phys. **17**, 30904 (2015).
[52]T. V. Tscherbul and P. Brumer, J. Phys. Chem. A **118**, 3100 (2014).
[53]A. Montoya-Castillo, T. C. Berkelbach, and D. R. Reichman, J. Chem. Phys. **143**, 194108 (2015).
[54]K. Blum, *Density Matrix Theory and Applications* (Springer Science & Business Media, 2012).
[55]H.-P. Breuer and F. Petruccione, *The Theory of Open Quantum Systems* (Oxford University Press, 2007).
[56]R. Alicki and K. Lendi, *Lecture Notes in Physics* (Springer, 2007), Vol. 286.
[57]T. P. Altenmüller, Z. Phys. D: At., Mol. Clusters **34**, 157 (1995).
[58]Z. S. Sadeq and P. Brumer, J. Chem. Phys. **140**, 074104 (2014).
[59]S. Mukamel, *Principles of Nonlinear Optical Spectroscopy* (Oxford University Press, New York, 1999).
[60]M. O. Scully and M. S. Zubairy, *Quantum Optics* (Cambridge University Press, 1997).
[61]B. Balzer and G. Stock, Chem. Phys. **310**, 33 (2005).
[62]P. Campomanes, M. Neri, B. A. C. Horta, E. F. Rohrig, S. Vanni, I. Tavernelli, and U. Rothlisberger, J. Am. Chem. Soc. **136**, 3842 (2014).
[63]S. Axelrod and P. Brumer, "Multiple time scale open systems: Reaction rates and quantum coherence in model retinal photoisomerization under incoherent excitation," J. Chem. Phys. (submitted).